npj | climate and atmospheric science

Article

Published in partnership with CECCR at King Abdulaziz University

https://doi.org/10.1038/s41612-025-01150-5

Changes in atmospheric oxidants teleconnect biomass burning and ammonium nitrate formation

Damaris Y. T. Tan[1,2] ✉, Mathew R. Heal[2], Massimo Vieno[1], David S. Stevenson[3], Stefan Reis[1,2] & Eiko Nemitz[1]

Open biomass burning has major impacts on the Earth system, including on air quality via the emission of primary fine particulate matter ($PM_{2.5}$). Its effect on secondary inorganic $PM_{2.5}$ formation is comparatively little investigated. Simulations with the EMEP MSC-W WRF atmospheric chemistry transport model reveal that global biomass burning emissions lead to elevated annual mean ammonium nitrate (NH_4NO_3) concentrations in densely populated regions where biomass burning mostly does not occur. These regions include eastern USA, northwestern Europe, the Indo-Gangetic Plain and eastern China, where NH_4NO_3 conditional on biomass burning emissions constitutes between 29% and 51% of the annual mean $PM_{2.5}$ conditional on biomass burning emissions. Biomass burning emissions of CO, NO_x (NO and NO_2) and volatile organic compounds perturb the HO_x (OH and HO_2) cycle globally, such that there is increased oxidation of anthropogenic NO_x to HNO_3. This results in additional contributions to local-scale secondary NH_4NO_3 in areas with high emissions of anthropogenic NO_x and NH_3. These teleconnections increase, by up to a factor of two, the contribution of biomass burning emissions to long-term $PM_{2.5}$ concentrations, which measurements alone cannot identify as an impact of biomass burning activity. This may become relatively more important as anthropogenic sources of $PM_{2.5}$ are reduced and as the wildfire component of biomass burning increases under climate change.

Wildfires and other forms of open biomass burning impact many facets of the Earth system, from radiative forcing and biodiversity, to air pollution and human health[1–3]. Wildfires, in particular, are an increasingly important influence on atmospheric composition. These are likely to increase in frequency, magnitude and intensity as a consequence of changes in climate and other factors such as population and land-use. Changes in their spatio-temporal patterns are also expected[1,4,5].

Here we use the terminology open biomass burning (BB) to refer to wildfires, prescribed fires and agricultural fires collectively. BB emits a range of trace gases, including carbon monoxide (CO), $NO + NO_2$ (NO_x) and ammonia (NH_3)[6]. Of particular relevance to human health, BB is also a major source of particulate matter with an aerodynamic diameter of less than 2.5 μm ($PM_{2.5}$). Due to its relatively short atmospheric lifetime (days to weeks), pyrogenic primary $PM_{2.5}$ is most abundant close to its source regions, typically on a scale of several hundred kilometres. This has been well explored on global and regional scales as part of fire inventories[7–10] and modelling and observational studies[1,2,11]. However, the formation of secondary $PM_{2.5}$ as a result of BB emissions — particularly in the context of air quality — is considerably less well investigated. As nations strive to comply with more stringent $PM_{2.5}$ targets, including aspirations to the WHO annual mean guideline[12] of 5 μg m^{-3}, the relative importance of BB-derived secondary $PM_{2.5}$ is increasing.

Most studies on the influence of BB on secondary $PM_{2.5}$ have focused on the formation of secondary organic aerosol[13–19], which can be estimated using marker compounds such as levoglucosan and potassium, or via aerosol mass spectra or optical properties[13,15,16,18]. Our focus here is on the influence of BB on secondary inorganic ammonium nitrate (NH_4NO_3) aerosol, which measurements cannot directly quantify. Previous work has tended to consider this only as part of case studies of individual BB events. For example, using in situ measurements and back-trajectory modelling of an episode of wildfire smoke reaching Athens in 2010, Diapouli et al. found elevated secondary inorganic aerosols, including a 0.26 μg m^{-3} increase in NH_4NO_3[18]. In modelling studies, Xing et al. found that BB-derived NH_4NO_3 contributed 32% and 78% to the total BB-derived $PM_{2.5}$ in

[1]UK Centre for Ecology & Hydrology, Penicuik, UK. [2]School of Chemistry, University of Edinburgh, Edinburgh, UK. [3]School of GeoSciences, University of Edinburgh, Edinburgh, UK. ✉e-mail: damtan@ceh.ac.uk; damaris.tan@ed.ac.uk

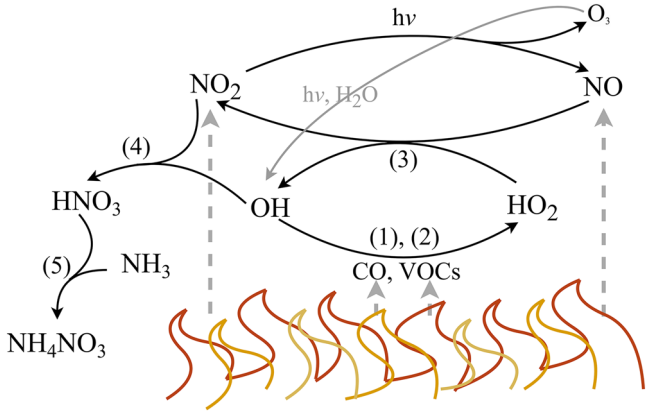

Fig. 1 | A simplified schematic of the HOx cycle in the context of BB emissions.

Yunnan Province, China, and other downwind areas respectively, during a 2015 episode of BB in peninsular Southeast Asia[20]; and Agarwal et al. found a 5−50% NH_4NO_3 contribution to BB-derived $PM_{2.5}$ during a 2016 pollution episode in the middle Indo-Gangetic Plain[21].

Central to the formation of secondary $PM_{2.5}$ is the OH + HO_2 (HO_x) cycle. Figure 1 shows a simplified schematic of the cycle relevant to the chemistry of BB emissions investigated here. BB primarily impacts the HO_x cycle via emissions of CO, volatile organic compounds (VOCs) and NO_x, through Reactions (1), (2) and (3), respectively. (In Reaction (2), VOCs are represented generically as RH, with R′ being a hydrocarbon intermediate with one less carbon than R.)

$$CO + OH \xrightarrow{O_2} CO_2 + HO_2 \quad (1)$$

$$RH + OH \xrightarrow{O_2} R' + CO_2 + HO_2 \quad (2)$$

$$HO_2 + NO \rightarrow NO_2 + OH \quad (3)$$

Changes in HO_x impact the oxidation of many compounds, including that of NO_x to nitric acid (HNO_3) (Reaction (4)), which in turn impacts on the formation of NH_4NO_3 (Reaction (5)).

$$OH + NO_2 \xrightarrow{M} HNO_3 \quad (4)$$

$$HNO_3 + NH_3 \rightleftharpoons NH_4NO_3 \quad (5)$$

The impact of BB on HO_x abundances has received only occasional previous attention, and again only in the context of episodes. In a modelling study of the 1997 Indonesian wildfires, Duncan et al. reported a net reduction in hydroxyl (OH) radical over the tropical Indian Ocean, primarily due to removal via CO[22]. Whilst the importance of this for subsequent tropospheric chemistry was identified, it was not elaborated on further.

Consequently, the aim of this study was to investigate the distribution and chemical drivers for the BB-induced formation of NH_4NO_3 globally, and on an annual-mean basis given that the health burden of exposure to $PM_{2.5}$ is dominated by its long-term concentrations rather than by episodes. We reveal the unexpected outcome that BB can enhance levels of NH_4NO_3 in densely populated areas considerably distant from locations of BB.

Results and discussion

BB, $PM_{2.5}$ and NH_4NO_3

The four panels of Fig. 2 show the 2019 global annual mean surface distributions of:

(a) $PM_{2.5}$(BB): the concentration of $PM_{2.5}$ conditional on BB emissions.
(b) $PM_{2.5}$(BB)/$PM_{2.5}$: the fraction of total $PM_{2.5}$ (from all sources) that is conditional on BB emissions.
(c) NH_4NO_3(BB): the concentration of fine NH_4NO_3 conditional on BB emissions.
(d) NH_4NO_3(BB)/$PM_{2.5}$(BB): the fractional contribution of fine NH_4NO_3 conditional on BB, with respect to the concentration of $PM_{2.5}$ conditional on BB.

We use the phrasing "conditional on BB emissions" to emphasise that these are aerosol components that would not exist without the BB but which do not all derive directly from BB emissions.

The black rectangles in each panel of Fig. 2 demarcate four regions of interest over (A) eastern USA, (B) northwestern Europe, (C) the Indo-Gangetic Plain and (D) eastern China. The bounding coordinates and surface area enclosed are listed in Supplementary Table C2. The selection of these boxes is based on the spatial pattern observed in panel (d) and are used simply to provide indicative average values for the magnitude of BB-derived contributions to secondary inorganic $PM_{2.5}$ surface concentrations over locations of higher population density. As panels (c, d) show, the largest contributions occur almost exclusively in the northern hemisphere. The means, maxima and minima of the variable values across each region are summarised in Supplementary Table C3.

Panels (a, b) of Fig. 2 highlight that BB activity in areas of western Canada and Alaska, Central and South America, Central Africa, Siberia, Southeast Asia and southeastern Australia made large contributions to annual mean surface $PM_{2.5}$ in 2019. This is consistent with the areas of high BB emissions in 2019 shown in Supplementary Fig. A3. The concentrations of $PM_{2.5}$ conditional on BB in regions A–D on an annual mean basis range between 1.2 μg m^{-3} in region A and 3.1 μg m^{-3} in region C, but are much larger during individual pollution episodes[21]. The contribution of $PM_{2.5}$ conditional on BB to total $PM_{2.5}$, again on an annual mean basis, ranges from 3.5% in region D to 8.7% in region B. Whilst these values are relatively small, processes conditional on BB nevertheless contribute an important proportion of $PM_{2.5}$ when considering the need to reduce $PM_{2.5}$ towards the WHO 2021 annual $PM_{2.5}$ guideline value[12] of 5 μg m^{-3}. As nations implement more stringent air quality mitigation, the relative importance of $PM_{2.5}$ conditional on BB will increase, much of which is outside national policy control.

Panels (c, d) demonstrate that NH_4NO_3(BB) can be a major secondary component of $PM_{2.5}$(BB) but has a very different global spatial pattern compared to panels (a, b). Regions A–D stand out in particular, with NH_4NO_3 contributing 29%, 51%, 36% and 47% respectively, to the total $PM_{2.5}$ enhancement conditional on BB ($PM_{2.5}$(BB)). (In all these regions the other major components of $PM_{2.5}$(BB) are primary and secondary organic matter).

Our mean values for the contribution of NH_4NO_3 conditional on BB to $PM_{2.5}$(BB) over regions A–D are similar to the percentages reported by Xing et al.[20] and Agarwal et al.[21]. However, it must be remembered that these authors investigate short pollution episodes linked to relatively local agricultural burning, whereas we present annual averages and include the impacts of BB at large distances from sources and occurring through different processes.

Both the spatial pattern and the magnitude of this secondary inorganic component of $PM_{2.5}$ conditional on BB is unexpected, particularly as regions A, B and D are not areas of large-scale fire activity (see Supplementary Fig. A3). We now explore the chemistry associated with these long-range effects of BB emissions.

BB and HO_x

Figure 3 shows the changes in 2019 annual mean surface concentrations of the OH and hydroperoxyl (HO_2) radicals attributed to all BB emissions (column 1), NO_x emitted from BB (column 2), CO emitted from BB (column 3) and VOCs emitted from BB (column 4).

Figure 3a shows that BB emissions lead to both decreases (blue colours) and increases (red colours) in annual mean surface OH concentrations. The

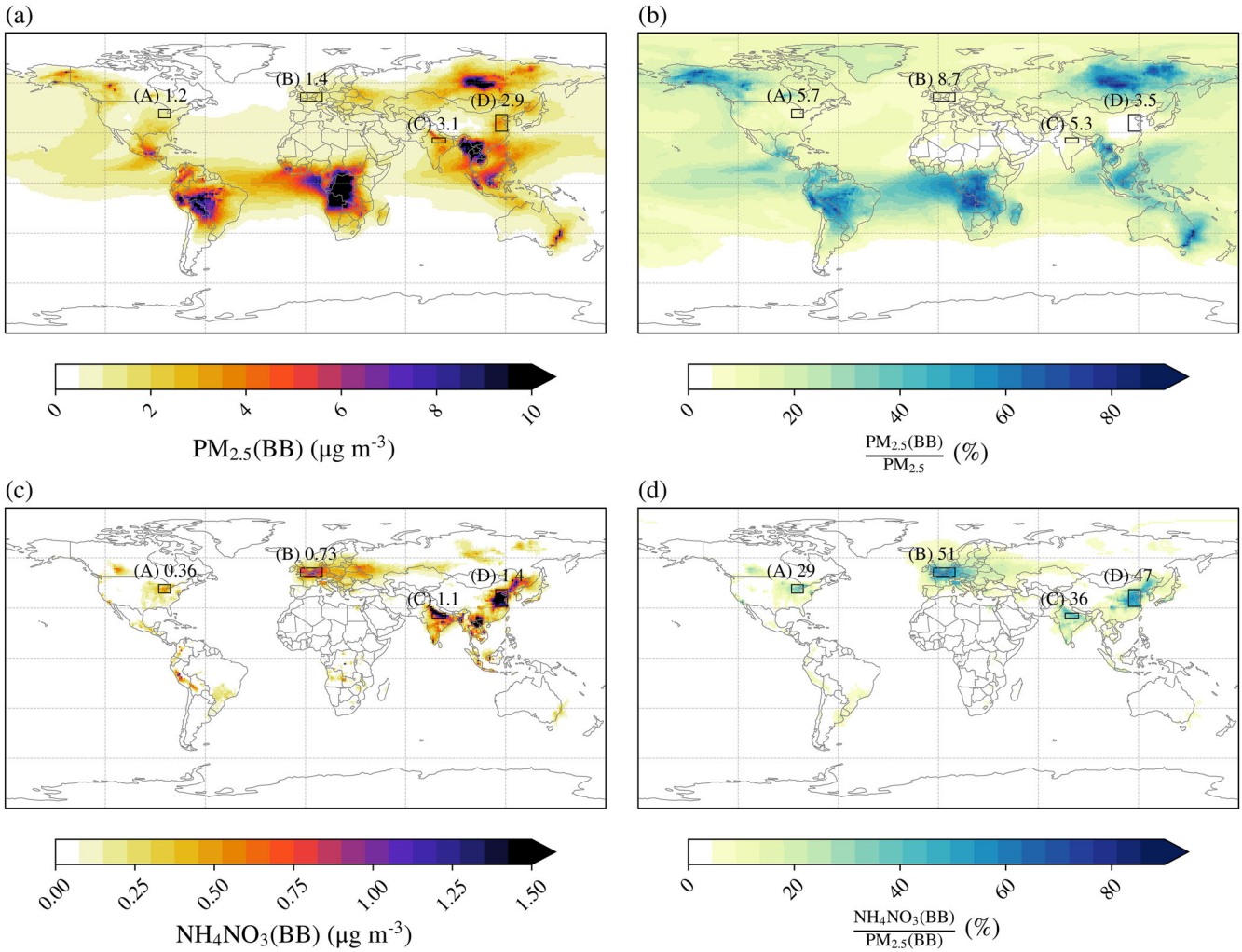

Fig. 2 | 2019 annual mean surface $PM_{2.5}$ concentrations conditional on BB. **a** $PM_{2.5}$(BB), the concentration of $PM_{2.5}$ conditional on BB emissions. **b** The percentage contribution to total $PM_{2.5}$ (from all sources) of $PM_{2.5}$ conditional on BB. **c** NH_4NO_3(BB), the concentration of fine NH_4NO_3 conditional on BB emissions. **d** The percentage contribution of fine NH_4NO_3 conditional on BB to $PM_{2.5}$(BB). The numbers on each panel are the mean values (in the units of the relevant legend) for the black rectangles positioned over high population areas in (A) eastern USA, (B) northwestern Europe, (C) the Indo-Gangetic Plain, and (D) eastern China (see Tables C2 and C3 for details).

decreases occur particularly over the oceans, and the increases occur over areas associated with large-scale BB (see map in Supplementary Fig. A3) and the highlighted regions B–D.

The decreases in OH surface concentrations due to BB are largely explained by the impact of pyrogenic CO on OH shown in Fig. 3c, in which pyrogenic CO converts OH to HO_2 via Reaction (1). The resultant increase in HO_2 is shown in Fig. 3g. This reaction dominates over the oceans, particularly shipping lanes, and illustrates the long-range impact of BB emissions on HO_x that is consequent on the relatively long lifetime (months) of CO. This is consistent with the > 20% reduction in OH over the tropical Indian Ocean through reaction with CO from BB and other BB-related mechanisms reported by Duncan et al.[22]. In some areas, for example over shipping lanes and large areas of the northern hemisphere, pyrogenic VOCs also contribute to this reduction in OH via Reaction (2). This is shown in Fig. 3d, with the resultant increase in HO_2 in Fig. 3h.

The increased OH surface concentrations shown in Fig. 3a are explained by the cumulative effect of pyrogenic NO_x, pyrogenic CO and pyrogenic VOCs in high NO_x areas (see maps of NO_x emissions and concentrations in Supplementary Fig. A2). The impact of pyrogenic NO_x on OH is shown in Fig. 3b, and is due to the reaction between BB emissions of NO and HO_2 to form OH (Reaction (3)). Since atmospheric NO_x itself has a relatively short lifetime (hours to days), this effect is particularly evident in areas of high BB emissions. However, pyrogenic NO_x can be transported via other species such as peroxyacyl nitrate (PAN)[23] (see Supplementary Fig. C8), leading to the BB-induced increases in OH distant from active fire regions.

In areas closer to substantial fire activity (see Supplementary Fig. A3), increases in HO_2 concentrations occur as shown in Fig. 3f. This can be explained by pyrogenic NO_x causing increased production of photochemical ozone (O_3) and OH (solid grey arrow in Fig. 1), which in turn increases the oxidation of OH to HO_2. Elevated levels of OH in fresh wildfire plumes have also been ascribed to the emissions of nitrous acid (HONO) during BB[24]; however BB-derived HONO emissions were not included in these simulations. Together with the increase in HO_2 shown in Fig. 3g and h, this leads to an overall increase in BB-associated HO_2, as shown in Fig. 3e.

There is also a contribution of pyrogenic CO and pyrogenic VOCs to OH concentrations over high NO_x areas like regions A-D (Fig. 3c and d). The conversion of HO_2 to OH (Reaction (3)) in high NO_x regimes occurs faster than the conversion of OH to HO_2 (Reactions (1) and (2)), leading to the increase in OH despite the presence of pyrogenic CO and pyrogenic VOCs.

The above cumulative effect explains the majority of the change in OH concentrations caused by BB emissions shown over regions A–D in Fig. 3a. However, NO_x, CO and VOCs are intrinsically linked through the HO_x cycle, leading to non-linear interactions that the simple BASE – NBBNOx, BASE – NBBCO and BASE – NBBVOC calculations cannot account for; i.e.

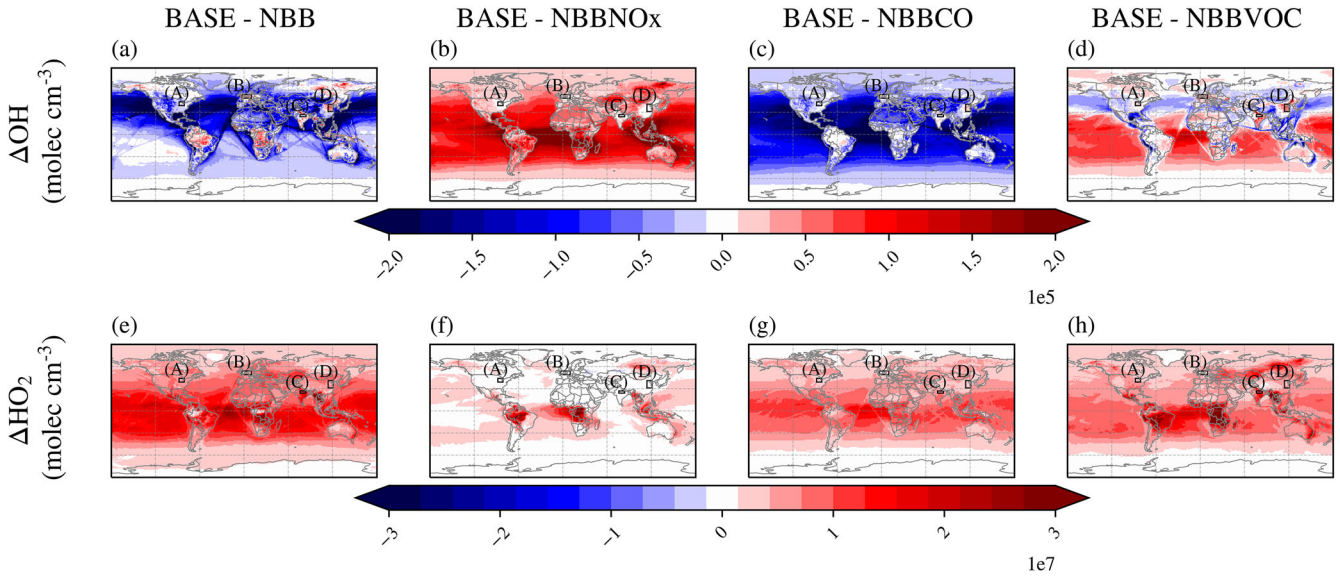

Fig. 3 | 2019 annual mean changes in surface HO_x concentrations conditional on BB. Surface concentrations of OH (**a**–**d**) and HO_2 (**e**–**h**) attributed to all open biomass burning (BB) emissions (**a**, **e**), NO_x emitted from BB (**b**, **f**), CO emitted from BB (**c**, **g**), and VOCs emitted from BB (**d**, **h**). The columns were calculated via BASE – NBB, BASE – NBBNOx, BASE – NBBCO and BASE – NBBVOC respectively. The four black rectangles are positioned over the same high population areas in eastern USA, northwestern Europe, the Indo-Gangetic Plain, and eastern China shown in Fig. 2.

superimposing panels (b–d) does not exactly reproduce panel (a). For example, HO_2 produced via pyrogenic CO and VOCs can react with pyrogenic nitric oxide (NO) as in Reaction (3), further enhancing the production of OH attributed to BB. This is not observed in panels (b–d) as it requires the presence of both pyrogenic CO and/or VOCs and pyrogenic NO_x.

From HO_x to NH_4NO_3

Figure 3 shows that BB emissions lead to a global increase in HO_2 surface concentrations, while OH surface concentrations generally decrease (with the exceptions already highlighted). As the changes in HO_2 surface concentrations due to BB emissions are around two orders of magnitude greater than those in OH, the net effect of BB emissions is to increase surface HO_x concentrations everywhere, as shown in Fig. 4a.

A distinction must again be made between regions with high BB emissions (see Supplementary Fig. A3) and regions of high anthropogenic NO_x and NH_3 emissions such as the highlighted regions A–D (see Supplementary Fig. A2). These are considered separately.

Over areas with substantial BB activity, Fig. 4b shows that BB causes a net increase in NO_x concentrations due to the direct NO_x emissions from the BB. Some of these direct BB emissions of NO_x are oxidised to form HNO_3 (Reaction (4)), as shown in Fig. 4c. Ammonia is also directly emitted from BB, as Fig. 4d confirms.

Conversely, in many areas of concentrated population and agriculture in the northern hemisphere, the effect of BB emissions is to decrease surface NO_x concentrations (Fig. 4b). These areas of decreased NO_x include the four regions of interest marked A–D on Figs. 2–4. In these areas, the increased HO_x brought about by BB emissions (Fig. 4a) enhances the oxidation of anthropogenic NO_x to HNO_3, which, through its equilibrium with NH_3 (Reaction (5)), yields the increased concentrations of NH_4NO_3 shown in Fig. 2d. Some of the additional HNO_3 formed remains as gaseous HNO_3 as shown in Fig. 4c.

This effect of BB emissions on NH_4NO_3 formation is particularly evident in regions A–D, which are areas of simultaneously high anthropogenic NO_x and NH_3 emissions (see Supplementary Fig. A2). In regions B and D the NH_3 emissions removed through the reaction with HNO_3 are predominantly anthropogenic, indicated by the reductions in NH_3 concentrations in Fig. 4d. Region C, while still an area of high anthropogenic NH_3 emissions, shows a net increase in NH_3 conditional on BB. Here it must be that removal of anthropogenic NH_3 is outweighed by increases in NH_3 from local BB emissions. Region A shows a response of surface NH_3 concentrations to BB emissions that is intermediate to the responses in the other regions highlighted.

Xing et al.[20] have previously emphasised the importance of oxidant concentrations for formation of NH_4NO_3 conditional on BB emissions. However, they also report that a major proportion of BB-derived NH_4NO_3 is attributed to direct pyrogenic NH_3 emissions, particularly in downwind areas. While direct NH_3 emissions from BB may play a key role in NH_4NO_3 formation at a regional scale, this is dependent on regional conditions such as proximity to the BB source, and the proportion of NH_3 derived from BB compared with other sources (predominantly agricultural). Globally, and on an annual-mean basis, our results suggest that NH_3 emitted directly from BB is only a minor contributor, especially over areas substantially removed from BB activity. This is, firstly, because of the relatively short lifetime of NH_3 (~1 day[25,26]) and consequent little long-range transport, and secondly, because of the very large agricultural NH_3 emissions in regions A–D.

Significance and caveats

Ultimately, it is the combination of global changes in atmospheric oxidant concentrations induced by pyrogenic NO_x, pyrogenic CO and pyrogenic VOCs, interacting with anthropogenic NO_x and agricultural NH_3 emissions in regions strongly associated with both, that leads to the unexpected hotspots of NH_4NO_3 conditional on BB revealed in Fig. 2c. This has direct consequences on the efforts to reduce exposure to annual mean $PM_{2.5}$ in these highly populated areas. As the formation of this NH_4NO_3 depends on the local emissions of NO_x and NH_3 as well as the long-range transport of BB-related emissions, it cannot be attributed to any single one of these three contributors. This is why we use the phrasing "conditional on biomass burning" rather than "from biomass burning" throughout this paper when referring to those primary and secondary aerosol components that would not exist without the BB.

Our findings illustrate the power of atmospheric chemistry transport models (ACTMs) to reveal the complex relationship between source and receptor regions that measurements alone cannot. Measurements would attribute any NH_4NO_3 exclusively to regional NH_3 and NO_x emissions, overlooking global BB as an important contributing factor. As a corollary, this study emphasises the need to constrain regional ACTM runs with global model runs that take into account global BB emissions.

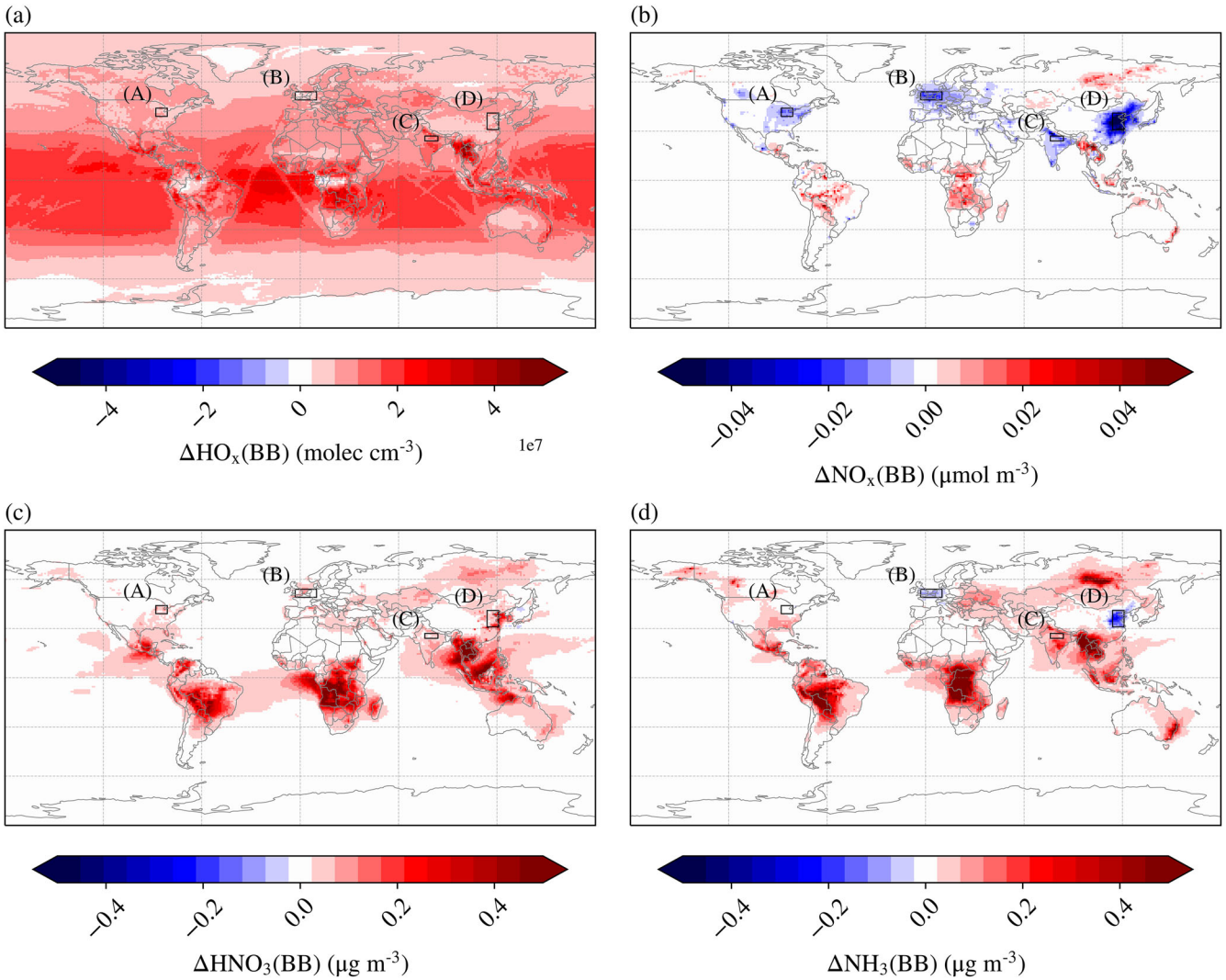

Fig. 4 | 2019 annual mean changes in surface concentrations conditional on BB. The impact of BB emissions on **a** HO_x, **b** NO_x, **c** HNO_3, and **d** NH_3. All concentration changes were computed by subtracting the NBB model run from the BASE model run. The four black rectangles are positioned over the same high population areas in eastern USA, northwestern Europe, the Indo-Gangetic Plain and eastern China shown in Fig. 2.

The chemistry of the atmosphere is complex so it is not possible to account for all effects observed in the figures shown here via one simple mechanism. Other changes in chemistry due to BB emissions will change other aspects of atmospheric chemistry, for example via O_3 chemistry. Additional factors also play a role, such as meteorological influences on precursor gas and particle deposition, atmospheric components such as mineral dust and sea salt, and factors influencing gas-particle partitioning such as water content, temperature and acidity[27].

The EMEP MSC-W model is a robust and well-tested model, but the exact magnitudes of the simulated values are highly dependent on the particular BB emissions dataset used (notably the ratio of NO_x, CO and VOCs), as well as the particular anthropogenic emissions, chemical scheme and meteorological model. Sensitivity experiments suggest that whilst these factors are important for precise quantification, the essential chemistry and findings presented here remain the same. For example, using different meteorological reanalysis data produced the same effects with different numerical values. Reducing BB emissions (FINNv2.5) by 10% reduced absolute values in Fig. 2a and c by 8−11%. Using FINNv1.5 reduces the absolute values in Fig. 2a and c by about two-thirds (consistent with FINNv1.5 emissions being > 50% lower than FINNv2.5 emissions[7]). Crucially, however, in both cases the percentage contributions of NH_4NO_3 shown in Fig. 2d remain the same.

It is also important to note that only plots of surface concentrations are shown here, whereas in reality BB emissions impact concentrations in three dimensions. However, vertical distributions of the species considered here (Supplementary Fig. C8) indicate that the secondary NH_4NO_3 formation we report is predominantly a near-surface effect. This is because NH_3 is emitted from the surface, and the reaction with HNO_3 is fast, so the bulk of NH_4NO_3 is also formed close to the surface.

Overall, the model results presented here clearly demonstrate an unexpected, yet important, long-range impact of BB emissions on a secondary inorganic component of $PM_{2.5}$ which is not normally correctly attributed when assessing the impact of global BB on particulate matter.

Methods

Model setup

Simulations for 2018 and 2019 were conducted using the global version of the European Monitoring and Evaluation Programme Meteorological Synthesizing Centre — West (EMEP MSC-W) rv4.36 Eulerian ACTM[28]. Only output for 2019 was used, to allow for spin-up of long-lived species. 2019 was a typical year for BB globally, albeit with slightly greater than average emissions (with the exception of temperate North America)[7].

The ACTM was driven by meteorology from the Weather Research and Forecast (WRF) model v4.2.2 at 1° × 1° horizontal resolution[29], which

used reanalysis data from the US National Centers for Environmental Prediction (NCEP)/National Center for Atmospheric Research (NCAR) Global Forecast System (GFS) and Newtonian nudging of wind vectors and temperature every 6 hours at 1° resolution[30].

Anthropogenic emissions were taken from the Task Force on Hemispheric Transport of Air Pollution (HTAP) v2 inventory for 2010 (regridded to 1° × 1° resolution)[31,32], which were the most recently available at the time of this work. The impact of this is discussed in Supplementary Section A. Emissions of isoprene and other biogenic VOCs from vegetation, NO_x from lightning and soil, marine dimethyl sulphide (DMS), and wind-derived dust and sea salt are all linked to the meteorological year and simulated as reported in Simpson et al.[28] and model update reports[33].

The EMEP MSC-W model uses the EmChem19 chemical scheme for gas-phase chemistry[34] and the Model for an Aerosol Reacting System (MARS) for inorganic aerosol thermodynamics[35]. The 1-D volatility basis set approach is used for secondary inorganic aerosol (SOA) formation, ageing and phase partitioning, with five volatility bins (effective saturation concentration C^* mid-points = 0.1, 1, 10, 100, 1000 μg m^{-3})[36,37]. Primary organic aerosol (POA) is treated as non-volatile and inert, as is assumed by emissions inventories[28].

Model output includes hourly gaseous and aerosol concentrations for 21 vertical levels between the surface and the tropopause. The lowest model layer has a height of ~48 m, and modelled air pollutant concentrations described here as surface concentrations have been adjusted to correspond to 3 m above the surface[28].

$PM_{2.5}$ is calculated as the sum of the fine (< 2.5 μm) fractions of sulfate (SO_4^{2-}), nitrate (NO_3^-), ammonium (NH_4^+), organic matter (OM), sea salt, windblown dust, road dust, elemental carbon (EC), ash and a remaining primary component. We do not include a water component to avoid ambiguity about how much water is associated with each $PM_{2.5}$ constituent.

BB emissions

BB emissions were obtained from the Fire INventory from NCAR (FINN) v2.5, which uses fire detections from both Moderate Resolution Imaging Spectroradiometer (MODIS) and Visible Infrared Imaging Radiometer Suite (VIIRS)[7,38]. The latter yields fire detection down to 375 m resolution. FINNv2.5 provides daily estimates of aerosol and trace gas emissions from BB globally at 0.1° × 0.1° resolution, calculated using burned area from active fire detections. In EMEP MSC-W rv4.36, these emissions are evenly distributed over the lower model layers up to 800 hPa[39].

Sensitivity experiments

The following five model experiments were carried out:

1. 'BASE': the base run with all emissions included.
2. 'NBB': no BB emissions from FINNv2.5.
3. 'NBBNOx': no BB NO_x emissions from FINNv2.5.
4. 'NBBCO': no BB CO emissions from FINNv2.5.
5. 'NBBVOC': no BB VOC emissions from FINNv2.5.

Concentrations conditional on BB emissions were computed by subtracting the NBB run from the BASE run. Concentrations attributed to BB emissions of CO, NO_x and VOCs individually were calculated by subtracting respectively the NBBCO, NBBNOx, and NBBVOC runs from the BASE run.

The sensitivity of these results to both BB and anthropogenic emissions was tested by carrying out model runs with a 33% reduction in anthropogenic CO emissions, a 10% reduction in BB emissions, and with the older FINNv1.5 BB emissions dataset (fire detections down to ~1 km resolution and other significant changes in methodology compared to v2.5[7,40]).

Model evaluation

The EMEP MSC-W model is widely used for air quality studies and its performance is regularly evaluated against measurements[33,41,42]. Its ability to simulate NH_4NO_3 and its precursors is discussed in Supplementary Section B.1. Its ability to simulate CO, as a marker of long-range transport of emissions relevant to this study, was additionally investigated here as described in Supplementary Section B.2. The model captures the seasonal cycles of CO well although it systematically overestimates CO by 20−100% compared to measurements. The sensitivity experiments reducing anthropogenic CO and BB emissions indicate that shortcomings in direct CO emissions are not the main reason for this bias. Instead, it likely originates from errors associated with other species involved in CO production such as VOCs[43]. The sensitivity experiments with reduced anthropogenic CO emissions had a negligible effect on the results presented here.

Data availability

EMEP MSC-W WRF model output presented in the figures of this paper is available at https://doi.org/10.5281/zenodo.15969976.

Code availability

EMEP MSC-W model code is available from the Norwegian Meteorological Institute GitHub pages (https://github.com/metno/emep-ctm). WRF model code is available from the Weather Research and Forecasting Model GitHub pages (https://github.com/wrf-model/WRF).

Received: 19 February 2025; Accepted: 23 June 2025;
Published online: 22 July 2025

References

1. United Nations Environment Programme. *Spreading Like Wildfire–The Rising Threat of Extraordinary Landscape Fires. A UNEP Rapid Response Assessment* (UNEP, 2022); https://www.unep.org/resources/report/spreading-wildfire-rising-threat-extraordinary-landscape-fires.
2. Keywood, M. et al. Fire in the Air: Biomass Burning Impacts in a Changing Climate. *Crit. Rev. Environ. Sci. Technol.* **43**, 40–83 (2013).
3. Xu, R. et al. Global, regional, and national mortality burden attributable to air pollution from landscape fires: a health impact assessment study. *Lancet* **404**, 2447–2459 (2024).
4. Jones, M. W. et al. State of wildfires 2023–2024. *Earth Syst. Sci. Data* **16**, 3601–3685 (2024).
5. Cunningham, C. X., Williamson, G. J. & Bowman, D. M. Increasing frequency and intensity of the most extreme wildfires on Earth. *Nat. Ecol. Evol.* **8**, 1420–1425 (2024).
6. Andreae, M. O. Emission of trace gases and aerosols from biomass burning–an updated assessment. *Atmos. Chem. Phys.* **19**, 8523–8546 (2019).
7. Wiedinmyer, C. et al. The Fire Inventory from NCAR version 2.5: an updated global fire emissions model for climate and chemistry applications. *Geosci. Model Dev.* **16**, 3873–3891 (2023).
8. Kaiser, J. W. et al. Biomass burning emissions estimated with a global fire assimilation system based on observed fire radiative power. *Biogeosciences* **9**, 527–554 (2012).
9. Giglio, L., Randerson, J. T. & van der Werf, G. R. Analysis of daily, monthly, and annual burned area using the fourth-generation global fire emissions database (GFED4). *J. Geophys. Res. Biogeosci.* **118**, 317–328 (2013).
10. van der Werf, G. R. et al. Global fire emissions estimates during 1997–2016. *Earth Syst. Sci. Data* **9**, 697–720 (2017).
11. Whaley, C. H. et al. HTAP3 Fires: towards a multi-model, multi-pollutant study of fire impacts. *Geosci. Model Dev* **18**, 3265–3309 (2025).
12. World Health Organization. *WHO global air quality guidelines: particulate matter ($PM_{2.5}$ and PM_{10}), ozone, nitrogen dioxide, sulfur dioxide and carbon monoxide* (World Health Organization, 2021).
13. Vasilakopoulou, C. N. et al. Rapid transformation of wildfire emissions to harmful background aerosol. *npj Clim. Atmos. Sci.* **6**, 218 (2023).
14. Theodoritsi, G. N. et al. Biomass burning organic aerosol from prescribed burning and other activities in the United States. *Atmos. Environ.* **241**, 117753 (2020).
15. Budisulistiorini, S. H. et al. Dominant contribution of oxygenated organic aerosol to haze particles from real-time observation in

Singapore during an Indonesian wildfire event in 2015. *Atmos. Chem. Phys.* **18**, 16481–16498 (2018).
16. Vakkari, V. et al. Major secondary aerosol formation in southern African open biomass burning plumes. *Nat. Geosci.* **11**, 580–583 (2018).
17. Gunsch, M. J. et al. Ubiquitous influence of wildfire emissions and secondary organic aerosol on summertime atmospheric aerosol in the forested Great Lakes region. *Atmos. Chem. Phys.* **18**, 3701–3715 (2018).
18. Diapouli, E. et al. Physicochemical characterization of aged biomass burning aerosol after long-range transport to Greece from large scale wildfires in Russia and surrounding regions, Summer 2010. *Atmos. Environ.* **96**, 393–404 (2014).
19. He, Y. et al. Formation of secondary organic aerosol from wildfire emissions enhanced by long-time ageing. *Nat. Geosci.* **17**, 124–129 (2024).
20. Xing, L. et al. Impacts of Biomass Burning in Peninsular Southeast Asia on PM2.5 Concentration and Ozone Formation in Southern China During Springtime—A Case Study. *J. Geophys. Res. Atmos* **126**, e2021JD034908 (2021).
21. Agarwal, P., Stevenson, D. S. & Heal, M. R. Quantifying the dominant sources influencing the 2016 particulate matter pollution episode over northern India. *Environ. Sci. Atmos.* **4**, 655–669 (2024).
22. Duncan, B. N. et al. Indonesian wildfires of 1997: Impact on tropospheric chemistry. *J. Geophys. Res. Atmos.* **108**, 4458 (2003).
23. Zhai, S. et al. Transpacific Transport of Asian Peroxyacetyl Nitrate (PAN) Observed from Satellite: Implications for Ozone. *Environ. Sci. Technol.* **58**, 9760–9769 (2024).
24. Theys, N. et al. Global nitrous acid emissions and levels of regional oxidants enhanced by wildfires. *Nat. Geosci.* **13**, 681–686 (2020).
25. Bian, H. et al. Investigation of global particulate nitrate from the AeroCom phase III experiment. *Atmos. Chem. Phys.* **17**, 12911–12940 (2017).
26. Ge, Y., Vieno, M., Stevenson, D. S., Wind, P. & Heal, M. R. A new assessment of global and regional budgets, fluxes, and lifetimes of atmospheric reactive N and S gases and aerosols. *Atmos. Chem. Phys.* **22**, 8343–8368 (2022).
27. Nenes, A., Pandis, S. N., Weber, R. J. & Russell, A. Aerosol pH and liquid water content determine when particulate matter is sensitive to ammonia and nitrate availability. *Atmos. Chem. Phys.* **20**, 3249–3258 (2020).
28. Simpson, D. et al. The EMEP MSC-W chemical transport model—technical description. *Atmos. Chem. Phys.* **12**, 7825–7865 (2012).
29. Skamarock, W. C. et al. *A Description of the Advanced Research WRF Model Version 4*. *NCAR Tech. Note NCAR/TN-556+STR* (NCAR, 2019); http://library.ucar.edu/research/publish-technote
30. Saha, S. et al. The NCEP climate forecast system reanalysis. *Bull. Am. Meteorol. Soc.* **91**, 1015–1058 (2010).
31. HTAP. *EDGAR for HTAP v2* (HTAP, accessed 01 May 2024); https://edgar.jrc.ec.europa.eu/dataset_htap_v2
32. Janssens-Maenhout, G. et al. HTAP_v2.2: a mosaic of regional and global emission grid maps for 2008 and 2010 to study hemispheric transport of air pollution. *Atmos. Chem. Phys.* **15**, 11411–11432 (2015).
33. Fagerli, H. et al. Convention on Long-range Transboundary Air Pollution Co-operative programme for monitoring and evaluation of the lang-range transmission of air pollutants in Europe. *Norwegian Meteorological Institute* (2024). https://emep.int/publ/reports/2024/EMEP_Status_Report_1_2024.pdf.
34. Bergström, R., Hayman, G. D., Jenkin, M. E. & Simpson, D. *Update and Comparison of Atmospheric Chemistry Mechanisms for the EMEP MSC-W Model System-EmChem19a, EmChem19X, CRIv2R5Em, CB6r2Em, and MCMv3.3Em* (Norwegian Meteorological Institute, 2022). https://emep.int/publ/reports/2022/MSCW_technical_1_2022.pdf
35. Binkowski, F. S. & Shankar, U. The regional particulate matter model: 1. model description and preliminary results. *J. Geophys. Res. Atmos.* **100**, 26191–26209 (1995).
36. Ots, R. et al. Simulating secondary organic aerosol from missing diesel-related intermediate-volatility organic compound emissions during the Clean Air for London (ClearfLo) campaign. *Atmos. Chem. Phys.* **16**, 6453–6473 (2016).
37. Donahue, N. M., Robinson, A. L., Stanier, C. O. & Pandis, S. N. Coupled Partitioning, Dilution, and Chemical Aging of Semivolatile Organics. *Environ. Sci. Technol.* **40**, 2635–2643 (2006).
38. UCAR/NCAR/ACOM. *Fire Inventory from NCAR version 2 Fire Emission* (NCAR, accessed 3 May 2023); https://rda.ucar.edu/datasets/ds312.9/
39. Fagerli, H. et al. *EMEP Status Report 1/2023: Transboundary particulate matter, photo-oxidants, acidifying and eutrophying components* (Norwegian Meteorological Institute, 2023); https://emep.int/publ/reports/2023/EMEP_Status_Report_1_2023.pdf.
40. Wiedinmyer, C. et al. The Fire INventory from NCAR (FINN): a high resolution global model to estimate the emissions from open burning. *Geosci. Model Dev.* **4**, 625–641 (2011).
41. Ge, Y., Heal, M. R., Stevenson, D. S., Wind, P. & Vieno, M. Evaluation of global EMEP MSC-W (rv4.34) WRF (v3.9.1.1) model surface concentrations and wet deposition of reactive N and S with measurements. *Geosci. Model Dev.* **14**, 7021–7046 (2021).
42. van Caspel, W. E. et al. Implementation and evaluation of updated photolysis rates in the EMEP MSC-W chemistry-transport model using Cloud-*J* v7.3e. *Geosci. Model Dev.* **16**, 7433–7459 (2023).
43. Shindell, D. T. et al. Multimodel simulations of carbon monoxide: Comparison with observations and projected near-future changes. *J. Geophys. Res. Atmos.* **111**, D19306 (2006).

Acknowledgements

The authors acknowledge helpful discussions with particular members of the UK Centre for Ecology & Hydrology's air quality modelling group (Janice Scheffler, Yuanlin Wang, and Tomáš Liška) and the University of Edinburgh's 'Modelling and measuring atmospheric composition and air quality at Edinburgh' group (Hannah Bryant). This work has been supported by the UK Department for the Environment, Food and Rural Affairs (Defra) under Contract ECM-53210: Support for national air pollution control strategies (including studentship funding for D.Y.T.T.). This work was partially supported by the following UK Research and Innovation (UKRI) grants: the UKCEH National Capability for UK Challenges programme (NE/Y006208/1), the UKCEH National Capability for Global Challenges programme (NE/X006247/1) and the UKRI GCRF South Asian Nitrogen Hub (NE/S009019/1). The findings and discussions presented here are those of the authors and do not necessarily represent the views of the funders.

Author contributions

D.Y.T.T. performed model simulations, data analyses and wrote the text under supervision by M.R.H., M.V., D.S.S., S.R. and E.N.. M.R.H., D.S.S., S.R., and E.N. edited and commented on the text. For the purpose of open access, the author has applied a creative commons attribution (CC BY) licence to any author accepted manuscript version arising.

Competing interests

The authors declare no competing interests.

Additional information

Supplementary information The online version contains supplementary material available at https://doi.org/10.1038/s41612-025-01150-5.

Correspondence and requests for materials should be addressed to Damaris Y. T. Tan.